# High-Resolution Observations of Internal Wave Turbulence in the Deep Ocean

**Hans van Haren**

## Introduction

The dynamics of the ocean resembles that of the atmosphere in many respects. Both are basically driven by the heating of the sun and adjusted by the rotation of the Earth [1]. One crucial difference is that the atmosphere is cooled at a higher geopotential level than where it is heated, while the ocean is heated at its top. As warm air/water is generally less dense than cold air/water, the heating generates natural vertical turbulent convective motions in the atmosphere, as an effective heat engine [2], while the ocean is merely a heat transporter as its heat engine is very ineffective [3]. Thus, a large amount of potential energy is stored in the ocean, but it requires a mechanical energy source to transport the heat downward against the stable stratification. Although the stable stratification in the ocean interior is 1000 times less than the density difference between air and water across the ocean surface, vertical diapycnal exchange is considered weak. The weak exchange may seriously affect life in the ocean and the replenishment of nutrients to the photic zone, for example.

However, the turbulent exchange is not blocked but hampered. This is because the density stratification may support destabilizing shear to the point of marginal stability (e.g., [4]) and mechanical energy in the form of waves, just like at the ocean surface. With the 1000 times weaker stratification in the interior, 'internal waves' may grow to attain 100 m large amplitudes that go barely unnoticed at the surface. Although linear, sinusoidal waves transport momentum but not matter, nonlinear waves can break and generate irreversible turbulent diapycnal mixing. It is the paradox of Munk and Wunsch [3] that demonstrates the importance of the relatively small amount of kinetic energy put into internal waves that is crucial to

H. van Haren (✉)
Royal Netherlands Institute for Sea Research (NIOZ), Utrecht University, Den Burg, The Netherlands
e-mail: hans.van.haren@nioz.nl



M. G. Velarde et al. (eds.), *The Ocean in Motion*, Springer Oceanography,
https://doi.org/10.1007/978-3-319-71934-4_11

maintain the ocean stratification via turbulence exchange, i.e. to govern the 25,000 times larger potential energy input by the sun.

Sea floor topography is important in both the generation (e.g., [5–7]) and the breaking of internal waves (e.g., [8, 9]). Not only the topography around ocean basin's edges act as source/sink of internal waves but especially also the topography found in ridges, mountain ranges and seamounts distributed over the ocean floor. There is more underwater topography than on land. The main mechanical source interacting with the topography is the tidal motion, which carries about 70% of the internal wave energy on average [3]. Another prominent source is related with the rotation of the Earth and the geostrophic response to sudden changes, e.g., by the passage of atmospheric disturbances or by the collapse of fronts: Inertial motions [1, 10]. Although the general aspect ratio of large-scale vertical:horizontal ocean current components is 1:1000, or perhaps 1:100, an encounter with topography forces a relatively large vertical motion that sets the, initially flat and horizontal, layers of constant density into oscillatory movements. The thus generated internal waves can propagate in full three-dimensions 3D spatially. After interactions with waves at other frequencies, or currents, or topography, the dominant process still being unknown, the initially linear waves become nonlinear and break whereby dissipating their energy. The associated turbulence not only affects the ocean stratification but also the marine geology and chemistry, by resuspending sediment and redistributing suspended material, and marine biology by the redistribution of nutrients and oxygen.

As internal waves can propagate freely when their frequencies are between the inertial frequency f, of horizontal oscillatory motion with short vertical scale thus an important shear 'source', and the buoyancy frequency N, the natural frequency of vertical oscillatory motion governed by the stratification, they are rather slow waves compared to surface waves. Internal wave periods vary between about a day and hours (in the deep ocean) to minutes (in generally stronger stratified waters of shallow seas and near the ocean surface). Such a slow motion is associated with linear waves that go up and down regularly. Faster motions are found beyond the buoyancy scales where the transitions to turbulence are found. When turbulence is mainly induced by wave-breaking, fronts of deformed internal waves pass instrumentation fixed in space within minutes.

The wave-breaking is a complex process in which the two main mechanisms to stratified turbulence co-exist. Vertical current shear across thin interfaces leads to overturning of Kelvin Helmholtz billows or instabilities KHI (e.g., [11]). The wave-overturning leads to 'free' buoyancy driven convection turbulence of Rayleigh-Taylor instabilities of a collapse of unstable ('cold') fluid overlying less dense ('warm') water [12]. Both mechanisms relate in a complex manner, e.g., a convection column [13] leads to shear instabilities along its fringes [14] and shear-induced overturning leads to convection in its core [15]. In the ocean these processes are most developed above sloping bottom topography.

Although some topography-internal wave interaction processes are well described, such as internal hydraulic jumps or lee-wave formation over seamounts and ridges [16, 17] and frequent overturning from internal wave breaking over slopes steeper 'supercritical' than the internal tide slope (e.g., [18, 19], Sarkar 2016,

pers. comm.), others are puzzling. While laboratory experiments over uniform slopes suggest wave breaking on 'critical' bottom slopes that match the angle of internal wave propagation [20, 21], wave-breaking in the ocean is also observed away from critical slopes of the major internal wave frequency, mostly tides, e.g. [22]. Examples of the latter wave breaking is also observed to occur in areas where near-horizontal inertial motions are the dominant carrier wave like in the Mediterranean, or sub-inertial motions like in the Faeroe-Shetland Channel [23], or trapped waves like along the Rockall Bank. This suggests a sloshing motion importance for the generation of nonlinear waves leading to breaking [19].

Even if the precise process leading to nonlinear wave formation is unknown, or not known for every particular topographic region, the importance of internal wave breaking upon topography associates with the importance of 'boundary mixing' for the maintenance of ocean stratification, as suggested by Munk [24] and Munk and Wunsch [3]. Assuming a layer of 100 m of enhanced turbulence over topography in an ocean of average depth of 3,000 m, Armi [25] suggested a turbulent diffusivity of $K_z = 3 \times 10^{-3}\ m^2\ s^{-1}$ sufficient to maintain the necessary heat flux in the ocean interior. This was debated by Garrett [26] as a boundary layer in the classic sense of Ekman [27], even over sloping bottoms [28], is homogeneous and thus very inefficient in its mixing, unless a complex restratification mechanism is invoked. The debate was based on steady flows having time scales much longer than the inertial period, or actually $t \gg 1/f$. Microstructure profiler observations by, e.g., [29, 30] to within 0.3 m from the bottom above sloping topography in shallow seas and [31] in the deep ocean showed that the turbulent flux ($\propto$turbulence dissipation rate) does increase towards the bottom and, indirectly, evidences effective mixing or a mechanism to restratify the sloping 'bottom boundary layer'. Detailed moored temperature sensor measurements (e.g., [32]) indicate that internal wave breaking dominates bottom friction in turbulence generation over sloping topography. It is also the key mechanism in rapidly restratifying the near-bottom area, by transporting the mixed waters into the interior and by pushing the stratification to within a meter or so from the bottom on time scales of the order of the inertial time scale, or shorter. They alternate with sudden upslope propagating frontal bores [23, 33] reaching up to 100 m above and actually touching the bottom thereby creating large sediment resuspension resembling a desert dust storm. In essence, a bottom boundary layer is not observed over sloping topography, at least not in the classic sense.

A challenge to this view is the requirement of a near-bottom reduction of the heat flux in order to have an upslope motion close to the bottom balancing the interior downward turbulent heat transport [34]. Whilst the concept is well-posed, it remains to be established how close to the bottom the heat flux should be reduced for the mechanism to work. Perhaps, the adoption of the theorem of Prandtl that the length-scales of the largest turbulent overturns can never be larger than the distance to the bottom in a mixing length theory may not be adequate for flows with more than one characteristic velocity [35]. Prandtl did not consider wave breaking over sloping topography, but frictional shear-driven turbulent overturning over a solid boundary.

A method has yet to be found to properly parameterize such wave-breaking motions, in the context of the large-scale ocean circulation. One of the unknowns is to relate to the proper scaling of topography. As the term 'rough topography' [9, 31] is somewhat imprecise in quantification, it would be better to consider the slope angle, in relation with the internal wave angles for given stratification, and the length scales of the slope-determination in association with the internal wave length scales. Apart from such modeling constraints, an encouraging recent tracer-release experiment near the Mid-Atlantic Ridge integrated over yearlong periods showed upslope motions that can only be balanced by diffusivities of about $K_z = 5 \times 10^{-3}$ m$^2$ s$^{-1}$ (Ledwell 2017, pers. comm.). It will be shown in this paper that such values are within a factor of two similar to those determined from high-resolution temperature sensors moored in various deep-ocean topographic regions. Under conditions of very high Reynolds numbers in the ocean that are not achieved in laboratories and a tight temperature-density relationship, such observations prove adequate in quantifying internal wave turbulence because of many 1-Hz yearlong sampled realizations of true vertical profiles under very little mooring motion.

## Instrumentation and Data

### *Quantifying Internal Wave Turbulent Mixing: Lowered Instruments*

Most turbulence measurements in the ocean have been performed using free-falling (few free-ascending) microstructure profilers, either loosely tethered to the ship or freely operating. These profilers carry shear probes and fast-response temperature (sometimes also conductivity) sensors that more or less resolve the Kolmogorov scales of smallest turbulence dissipation overturns that are about 0.1–0.01 s in time and 0.001–0.01 m in space, under ocean conditions. For statistical reasons, the raw several 100 Hz sampled data are divided in blocks of a few seconds long to give estimates of turbulence dissipation rate and eddy diffusivity. The disadvantages of this instrumentation are its relatively slow vertical speed of about 0.7 m s$^{-1}$, its 1D profiling of essentially 3D physical processes and its costs: a full ocean depth apparatus requires financing over 0.5 million US dollars and not many exist in the community.

A simpler but more commonly useable method was proposed by Thorpe [36] to infer turbulence estimates from standard oceanographic Conductivity Temperature Depth CTD data. This shipborne equipment also collects vertical (1D) profiles of ocean quantities at a slightly higher speed of just under 1 m s$^{-1}$ while sampling at a rate of 24 Hz for modern equipment. The turbulence estimation method is by reordering vertical density profiles into statically stable ones and keeping track of the displacements. Thus after some averaging to reduce noise the larger energy-containing turbulent eddies are resolved but not the (Kolmogorov) dissipation scales. In essence this is not a problem, provided some assumptions are made.

The first assumption is that the overturning displacements d are related to the Ozmidov scales $L_O$ of largest overturns in stratified turbulence. As indicated by Thorpe [36], after suitable (rms) averaging this is true to within a constant ratio of $c_1 = L_O/d_{rms} = 0.8$. This value was empirically established by Dillon [37] as being a mean in a distribution of about one order of magnitude wide. The distribution reflects the various stages of turbulence development and the two principal turbulence processes of shear-induction and convection. Recently, the overturning method was challenged from numerical simulations showing that convection leads to an underestimate of the Ozmidov scale using the displacements. But, the high Reynolds number ($10^4$–$10^6$) turbulence in the stratified ocean is a mix of shear-induction and convection rendering the average ratio very close to 1 [38] and confirming Dillon's observations. The second assumption is to use a constant value $m_1 = 0.2$ for the mixing efficiency [39, 40]. As with the Ozmidov/Overturning scale ratio, this constant is a mean from a distribution of about one order of magnitude wide and thus requires some suitable vertical, horizontal and/or time averaging. The third assumption was not necessary to make for Thorpe [36] as he designed the method for use in lakes: It involves salinity and ship's motions. The disadvantages of using the overturning method in the ocean are the ship's motion by surface waves that are only partially compensated by a heave compensator and the contribution of salinity to density variations. Both require corrections to the raw data that approach the order of magnitude of turbulent overturns (e.g., [41–44]).

## *Quantifying Internal Wave Turbulent Mixing: Moored Instruments*

Instead of lowering instruments from a ship one can use Eulerian moored instrumentation fixed in space under water and have the flow go past it. Under the assumption that one can separate via 'Reynolds decomposition' the turbulent fluctuations from the 'mean flow', one may directly estimate the turbulent momentum and/or heat (mass) fluxes with suitable current and temperature (conductivity) measurement devices. Although stand-alone instrumentation is heavily limited by sufficient power supply, this method is reasonably successful for estimating momentum fluxes in shallow seas by a moored acoustic point source measurement device like the Nortek Vector in shallow seas almost resolving the dissipation scales (e.g., [45]). Resolving larger scales, moored acoustic profiling instrumentation, especially operating in pulse-coherent mode, estimates statistically significant momentum fluxes above 'flat' shallow sea floors with dominant tidal friction (e.g., [46, 47]) and sloping topography [30]. However, the method has seldom produced significant results from the deep ocean [48], possibly due to the lack of sufficient scatterers. Few attempts have been made to actually estimate heat (mass) fluxes, above sloping topography [48, 30]. It appeared difficult to match the acoustic current measurements in slanted beams with data from a chain of

temperature 'T'-sensors along its central axis. More principally, the Reynolds decomposition requirement of a spectral gap between mean flow and turbulence is not found in the ocean. The method was thus also found inadequate for the deep ocean.

## *Quantifying Internal Wave Turbulent Mixing: Moored High-Resolution T-sensors*

As an alternative, NIOZ developed high-resolution T-sensors to be moored with relatively many and supported by some current and pressure measurements. Initially T-sensors were connected via cables to a central data logger and power supply unit [22]. After considerable connection problems it was decided to work with stand-alone self-contained sensors [49]. The high-resolution <0.1 mK and high precision <0.5 mK sensors have a response time of 0.25 s in water and standard sample at a rate of 1 Hz (adjustable) for a duration of one year on one AA-battery. Typically, 100 sensors are taped to a plastic-coated steel cable of several 100 m long. This offers great flexibility and sensors have been taped at intervals between 0.04 and 16 m depending on the required configuration for study. This is adequate to resolve most of the stratified turbulence and internal wave overturning scales as mean Ozmidov scales are between 0.1 and a few 10's of meters while large-scale internal wave amplitudes reach 100 m. The steel cable is used to synchronize the sensor clocks so that a profile of up to 600 m long (tested) is measured within 0.02 s. Such a snapshot over this vertical range is not achievable using 0.7–1.0 m $s^{-1}$ free-falling or lowered profilers. The large number of sensors in a profile is also adequate to correct for sensor drift, which amounts about 1 mK/mo after aging. For an averaging period longer than the buoyancy period, but commonly taken longer than the inertial period to be sure, turbulent overturns cannot last and the mean ocean profile is statically stably stratified. Any remaining unstable deviations are thus instrumental (or salinity driven, see below) and need to be corrected. This is achieved by forcing the mean observed profile to a smooth, stable profile using a constant correction per sensor. In practice, an averaging period of 2–7 days is chosen for this local correction and repeated for different times in the (up to yearlong) record.

Considerable effort is put in improving the mooring design by minimizing its motions to obtain almost truly Eulerian measurements with negligible artifacts in the frequency range of interest. At NIOZ it is preferred to have all buoyancy near the top so that recovery after successful release of the bottom weight is smooth without entanglement of cables. As large-scale ocean currents are almost horizontally, the associated drag forces by any object obstructing the flow are nearly perpendicular to gravity (negative buoyancy). A balance of forces is thus impossible and the mooring will inevitably be deflected by a non-zero flow. We impose the criterion that the vertical deflection may never exceed half the distance between any of the instruments along the mooring line, so typically <0.5 m for a mooring with a string of 1-m

separated T-sensors. This is achieved by using thin cables of 0.005 or 0.006 m diameter that have breaking strengths >20,000 N. These cables are tensioned by up to 5,000 N using a weight of >500 kg and net buoyancy of 300 kg where currents reach 0.3–0.4 m $s^{-1}$. Mooring design is verified using Richard Dewey's software (University of Victoria, BC, Canada). The mooring motion is always monitored by mounting at least one current meter and pressure and tilt sensors.

The sensors are calibrated at NIOZ using a thermostatic bath with constant temperature levels to within $\pm 10^{-4}$ °C of their preset values. The calibrated and drift-corrected data are transferred to Conservative (~potential) Temperature ($\Theta$) values using the gsw-software described in [50]. As the ocean density is also determined by salinity besides temperature, several shipborne SeaBird-911 CTD-profiles are obtained near the mooring. The CTD-data are also used to establish the local temperature-density relationship for use of the moored T-sensor data as tracer for potential density anomaly variations $\delta\sigma_x$, referenced to the pressure level x/1000 dbar of the mooring (see for an example Fig. 1).

When the linear relationship is reasonably tight (relative error of about 1–10%), the constant gradient $\alpha = \delta\sigma_x/\delta\Theta$ indicates an apparent local thermal expansion

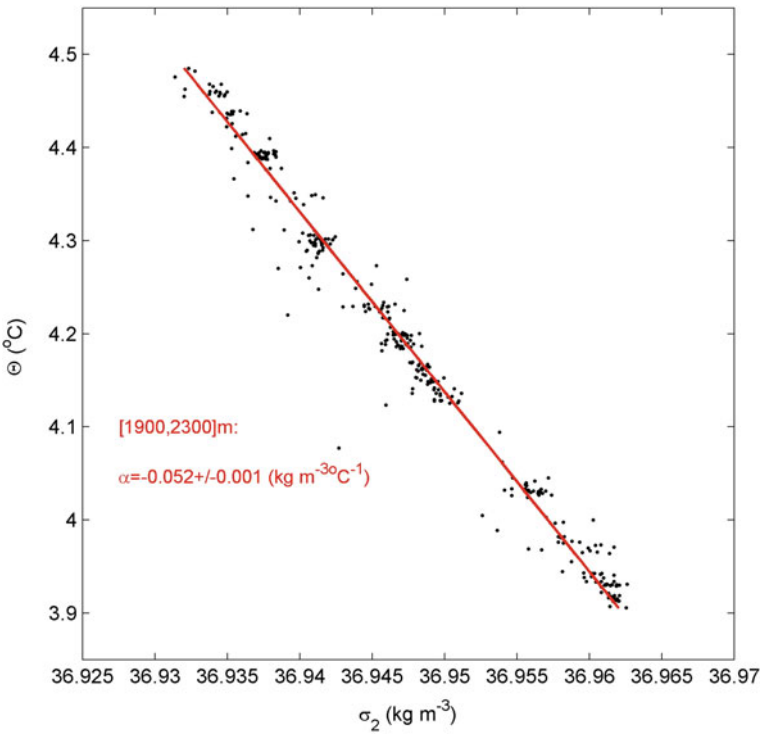


**Fig. 1** Conservative temperature-density anomaly relationship, referenced to 2,000 dbar from CTD-data obtained between 1,900 and 2,300 m near a T-sensor mooring on a slope of Mount Josephine NE Atlantic Ocean. The slope of the linear best-fit denotes the local apparent expansion coefficient

coefficient. If this relationship is not tight a relatively large or dominant contribution results of salinity to density variations, as around Mediterranean outflow of relatively warm and salty waters into a cooler and fresher Atlantic environment and in polar near-surface regions where the cold waters lead to ambient low thermal expansion coefficients, with added ice melt. This leads to intrusions of apparent overturns that can last longer than the buoyancy period. If intrusions are thus detectable they may qualitatively demonstrate turbulent motions, but quantitative turbulent information is no longer obtainable [51]. In contrast, the above relationship is always tight for data from lakes, where temperature exclusively dominates density variations, with the notion that the natural thermal expansion coefficient changes sign at about 4 °C.

With a tight temperature-density relationship, turbulence dissipation rate $\varepsilon = c_1^2 d^2 N^3$ and vertical eddy diffusivity $K_z = m_1 c_1^2 d^2 N$ are estimated from the T-sensor data using the method of Thorpe [36]. Here, N is computed from the reordered profiles. Figure 2 demonstrates the post-processing of splitting original 1 Hz profiles

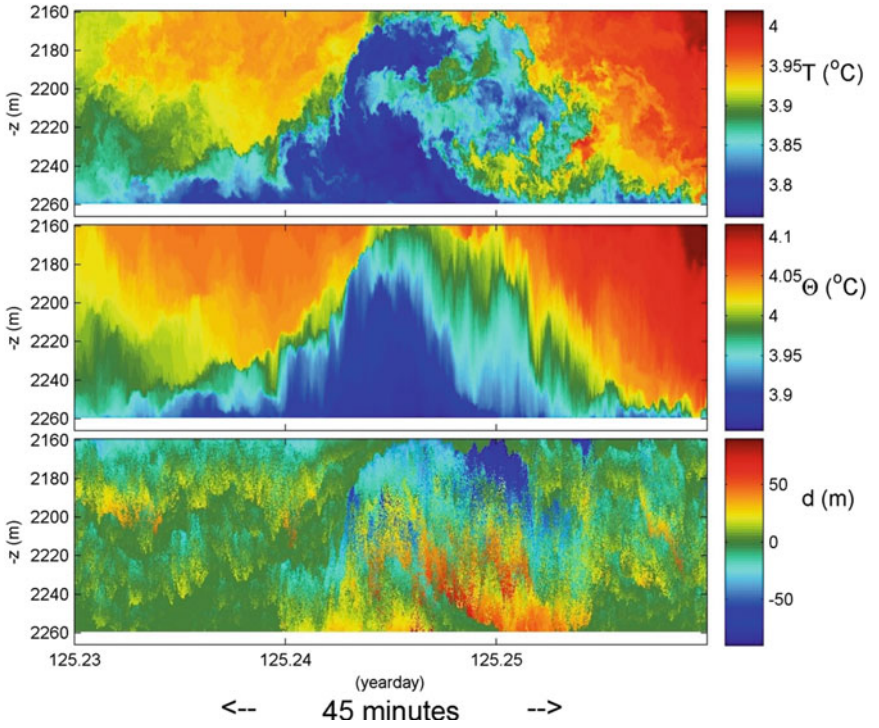


**Fig. 2** Detailed time-depth series example showing the split of observed moored T-sensor data into stably reordered profiles and the necessary displacements following the reordering. Forty-five minutes of data from an arbitrary 100-m tall overturn observed above Mount Josephine (the local water depth is at the level of the x-axis). **a** Original 1-Hz sampled temperature data using 100 independent sensors at 1 m vertical intervals starting at 6 m from the bottom. **b** Data from **a**. transferred to conservative temperature 'CT' and reordered to stable 1-Hz profiles. **c** Displacements between original CT-data and data from **b**

into reordered stable profiles and displacements. The 3D appearance (Fig. 2a) so well captured by 17th century clouds and landscape painters is completely absent in the flat 2D image (Fig. 2b) from which the turbulent displacements (Fig. 2c) are removed. The raw turbulence parameter estimates for every sensor and every (1 s) profile are averaged over depth, hereafter indicated by <…>, and time, indicated by […].

Thorpe [9, 36] proposed to average over individual turbulent overturns, but as smaller overturns exist in larger ones that even may exceed the range of moored sensors (cf., Fig. 2), it was decided to average over the full vertical range of T-sensors when it is equal to or less than 100 m [32]. Commonly, about 5% of the T-sensors show electronic or calibration problems and their data are linearly interpolated between neighboring sensors. This affects the turbulence parameter estimates by less than 10%, well within the standard error in the estimates due to the procedure.

## Observations

In the examples given in this section, areas are avoided where the temperature-density relationship is not tight. Although the locally established apparent thermal expansion coefficients vary considerably for different regions between 0.05 and 0.3 kg $m^{-3}$ $°C^{-1}$ and their 'tightness' between 1 and 10% of the mean value, the standard errors in turbulence parameters are always about a factor of two. This is equivalent to errors in microstructure profiler data after considerable and careful post-processing (Oakey 1991, pers. comm.). The factor of two error is confirmed by comparing moored T-sensor overturn estimates above a seamount slope with nearby shipborne lowered ADCP/CTD data estimates using Gregg [52]'s shear-scaling [32].

### *In the Open Ocean Far Away from Topography*

The stratified open ocean interior is permanently in motion, not merely by surface waves but especially also by internal waves with typical amplitudes of several tens of meters (e.g., [53–55]). The weakly turbulent motions are smooth, albeit not perfectly sinusoidal in shape, and have relatively large vertical coherent scales with near-zero phase difference over the range of thermistors ('local vertical mode-1'), at both tidal and near-buoyancy frequencies. Amplitudes vary continuously for motions within any particular finite frequency band; evidence of intermittency. Due to straining, the thickness of strongly stratified layers drops below 1 m, while weakly stratified layers can exceed tens of meters. In the Canary Basin [55], the mean Ozmidov scale $<L_O> \approx 0.4$ m (obtained from high-resolution shipborne CTD-data). The mean interior turbulence parameters are estimated as $[<\varepsilon>] \approx 10^{-9}$ $m^2$ $s^{-3}$ and $[<K_z>] \approx 2 \times 10^{-5}$ $m^2$ $s^{-1}$, which is equivalent to values estimated for other, upper 2000 m, open ocean regions [52] and for, e.g., the summer stratified

North Sea [4]. Such values are still 100 times larger than molecular diffusivity values and sufficient to explain, at least for shallow seas, the gradual warming of the near-bottom waters and the flux of nutrients into the photic zone to entirely support the late-summer phytoplankton bloom. This was found to be due to the stratification being marginally stable, with gradient Richardson number $Ri = N^2/|S|^2$ values of about $Ri = 0.5$, where the shear magnitude $|S|$ was composed of a quasi-permanent large inertial/tidal shear across largest stratification added with occasional small-scale internal wave shear. These turbulence values are also typical for a saturated internal wave field allowing for sparsely distributed turbulence [56], similar to surface wave white capping of a puff here and a puff there. However, according to Munk [24] they are insufficient to maintain the ocean stratification.

## *Above Sloping Topography*

When internal waves reach underwater topography like seamounts or ridges, the smooth motions turn into more irregular motions up to highly nonlinear and vigorous turbulent overturning, see for example Fig. 3. Although bottom slopes are on average just a few per cent and typical internal tide generating horizontal currents are 0.1 m $s^{-1}$, the impact of such currents and slopes is spectacular in their production of wave breaking. Turbulent overturning ranges from 10 to 100 m vertical scales (Figs. 2a and 3a).

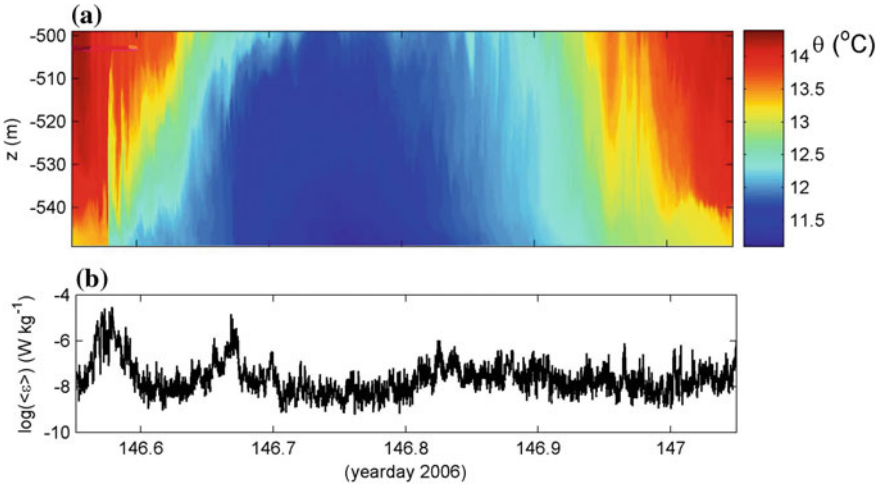


**Fig. 3** One tidal period of temperature observations using 101 temperature sensors above Great Meteor Seamount NE Atlantic Ocean, sampled at a rate of 1 Hz at 0.5 m vertical intervals, starting at 0.5 m from the bottom. **a** Time-depth image shows a tidal wave well exceeding the 50 m range of sensors. **b** Time series of the logarithm of turbulence dissipation rate inferred from the data in (**a**)

Especially the transition from warming to cooling phase of the large-scale carrier wave, associated with an upslope moving frontal bore, provides large turbulence peaking at $\varepsilon = 10^{-5} - 10^{-4}$ m$^2$ s$^{-3}$ and $K_z = 10^{-1} - 10^{0}$ m$^2$ s$^{-1}$ (Fig. 3b). The reordered stable stratification is characterized by very thin layering down to the lowest vertical resolution, in this case $\Delta z = 0.5$ m and much smaller than $<L_O> \approx$ 20 m. The layering approaches the bottom to within a meter just prior to a frontal passage by large interior overturns associated with relatively strong (0.1 m s$^{-1}$) downward motions [32]. The large convective overturns preceding the front are not so efficient in their mixing ($m_1 \approx 0.05$), but the near-bottom stratified layer forming the frontal bore is more efficient ($m_1 \approx 0.3 \leq 0.36$) than average [57]. The downdraught seems part of sharpening the turbulent bore moving up the slope.

The frontal bore itself is basically the only large overturn extending from the bottom upward, thus being important for sediment resuspension governed by 0.1 m s$^{-1}$ upward vertical current speeds [23]. Secondary instabilities are observed along its fringe, contributing to effective mixing [58]. Although turbulence associated with upslope propagating bores is always large, the intensity and precise extent vary every cycle of the carrier wave. The variations depend on the exact direction of bore propagation with respect to the main bottom-slope direction, the more upslope the stronger turbulent, and on the timing of arrival which varies over about 10% of the carrier wave period [59]. This variation in arrival time was attributed to variations in the background stratification which modify the paths of internal waves, and apparently also large-scale sub-inertial motions. Behind the front the trailing near-N waves also turn-over due to internal wave shear across the sharp interface, but in rapidly decreasing magnitude.

Averaged over time of a two-week period and over depth over the range of T-sensors gives $[<\varepsilon>] = 3 \pm 2 \times 10^{-7}$ m$^2$ s$^{-3}$, $[<K_z>] = 6 \pm 4 \times 10^{-3}$ m$^2$ s$^{-1}$ for $[<N>] = 5 \pm 3 \times 10^{-3}$ s$^{-1}$ above steep 'supercritical' slopes larger than the average internal tidal slope [32, 60]. These turbulence values are more than two orders of magnitude larger than estimated from ocean interior observations. Above less steep slopes, values are smaller, but even above slopes well less than the internal tide slope values are still about one order of magnitude larger than ocean interior values [60]. In the vertical above a supercritical slope, the latter low values are not observed up to 400 m above the bottom (Fig. 4) possibly due to the large extent of tidal motions that have top-trough excursions exceeding 100 m [61]. These observations tend to support microstructure profiler observations of the decrease of turbulence intensity to ocean interior values over a range of some 1000 m above sloping topography [31].

## *Interfacial Shear Instability Observations*

Although near sloping bottoms moored high-resolution T-sensors show largest turbulent overturning commonly in the form of frontal bores around the transition between warming and cooling phases of the large-scale carrier wave, time series of

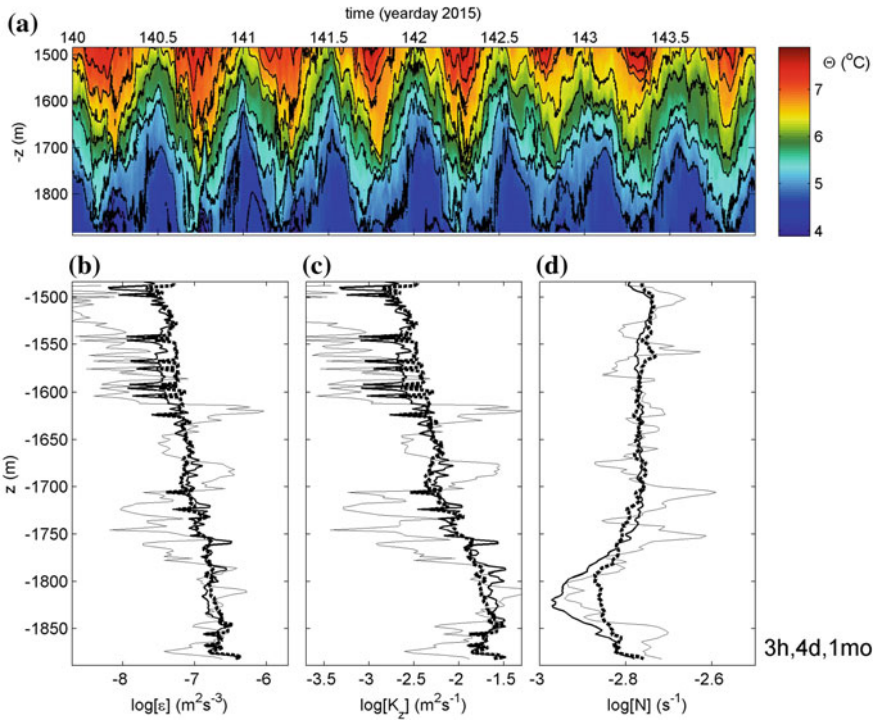


**Fig. 4** Four-day detail of temperature and inferred turbulence measurements above a super-critical slope for internal tides of Mount Josephine. **a** Conservative temperature time-depth series. **b–d** Full depth profiles of logarithms of time-averaged parameter values. One month averages are indicated by thick-dashed lines, four day (Fig. 4a) averages by thick-solid lines and 3 h averages by thin-solid lines. **b** Turbulence dissipation rate. **c** Vertical turbulence diffusivity. **d** Buoyancy frequency. After [61]

vertically averaged turbulence parameters show a variation over four orders of magnitude (Fig. 3b; e.g., [32]). This is typical for ocean turbulence and is also observed in vertical microstructure profiles (e.g., [39, 52, 31]). Apparent spiky variations over two orders of magnitude are not instrumental noise but indicative of individual overturns. Typical examples are trains of shear-induced KHI.

Trains of 5–10 KHI-overturns of about 5 m high are observed during the warming phase of the carrier wave, when the large-scale shear irregularly coincides with small-scale shear of internal waves near the local buoyancy frequency, see for example Fig. 5. The average $<L_O> \approx 1.8$ m and some overturn-billows are short-lived $O(10^1 - 10^2$ s). A more prominent train of 275 KHI-overturns in one day has been observed in the deep ocean around 4,500 m [62]. There at the entrance of the equatorial Romanche Fracture Zone of the Mid-Atlantic Ridge the tidal flow interacts with the large-scale flow driven by Antarctic Bottom Water plunging

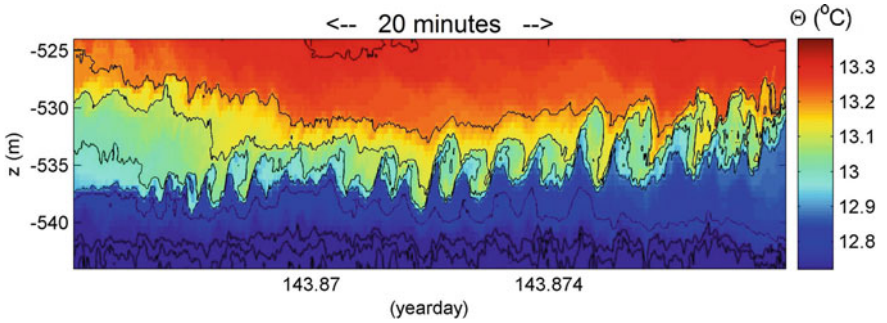


**Fig. 5** Twenty minutes and 20 m detailed example of the downslope propagating, warming phase of the internal tide observed using NIOZ3 T-sensors at 0.5 m vertical intervals near the top of Great Meteor Seamount

underneath North-Atlantic Bottom Water on its trajectory from the (south) western to the (north) eastern Atlantic Basin. When the tidal phase is in the direction of the large-scale flow, KHI have a vertical extent of 10–20 m. Half a tidal period later when the phase is directed against the large-scale flow KHI exceed 100 m vertically.

In all these KHI observed in the deep ocean, the roll-up stage of initial KH billows seems to be limited to half a turn, resembling half a Rankine vortex [44], before collapse. This is somewhat different than found in laboratory experiments (e.g., [63]) and numerical modelling (e.g., [15, 64]). As a rare exception, near-surface ocean optic [65] and acoustic observations [66] show a roll-up. Although the lack of deep-ocean observations of multiple scale billow roll-up is presently unknown, it may have to do with the large Reynolds numbers associated with the turbulent environment above sloping topography, causing a rapid collapse of the billows.

## *Some Temperature Statistics*

The largest overturns observed have a vertical length scale of about 100 m [62] and a time scale of just less than the buoyancy period [32]. The latter is commensurate the expectation that the buoyancy frequency is a natural scale separator between irreversible turbulent overturning and internal wave motions. As for the interpretation of (moored) temperature observations as a tracer for density variations, this information is useful to help distinguishing between genuine turbulent overturning and partially salinity compensated intrusions. The difference in shapes of apparent and turbulent temperature instabilities is also used for distinction.

A further distinction and determination is obtained from temperature scalar statistics [18]. In particular are we interested in the distinction between passive scalar, shear-dominated turbulence and active scalar, convection dominated

turbulence. The analysis confirms the differences sketched above between upslope cooling phase and downslope warming phase of the carrier wave. The former is consistent with passive scalar statistics but for the bottom half of a 100 m tall T-sensor array, while in the upper half also evidence is found of active scalar statistics. Likewise, the downslope phase is not exclusively dominated by passive scalar statistics. These observations confirm the notion that shear- and convection turbulence co-exist in the ocean, at least above sloping topography. In general strong intermittency is found during the downslope phase, while a clear inertial subrange of −5/3 spectral slope is observed during the upslope phase in particular in the lower 50 m above the bottom (cf., Fig. 6).

From extended statistics using nearly 500 sensors in a small-scale 3D mooring array of five lines 100 m long and 4 m apart horizontally, the inertial subrange is observed superposed by larger variability than expected from chi-squared statistics [67]. The observations suggest localized patches that are more coherent than their spectral surroundings (Fig. 6), and which are not found in open-ocean spectra. They may be due to intermittency, to convection in a shear-dominated environment, or to an interaction between turbulence and small-scale thin-layer internal wave motions: The precise mechanism is not known as the pattern is not yet resolved, except that their energy levels are found to be proportional to the tidal energy level as their peaks fall along a −2 spectral slope to within the 95% statistical significance level.

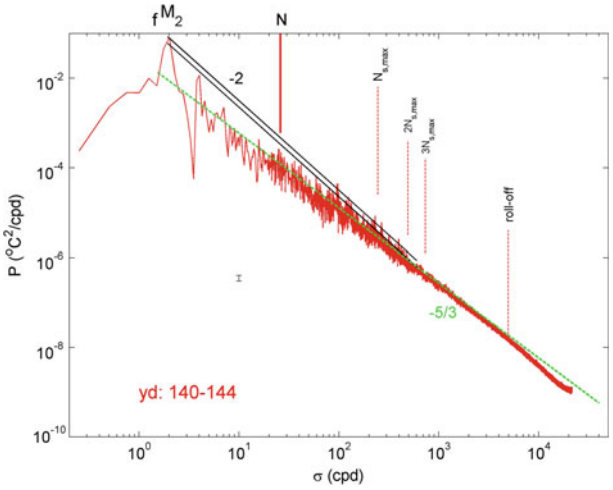


**Fig. 6** Temperature variance spectrum, an average of 442 near-raw periodograms for the Kaiser window tapered time series of a four-day turbulent period observed by independent T-sensors at a small-scale 3D (five line) mooring array above a super-critical slope of Mount Josephine. The data are sub-sampled at 0.5 Hz for computational reasons. Besides inertial (f) and semidiurnal lunar tidal ($M_2$) frequencies several buoyancy frequencies are indicated including four-day large-scale mean N and the maximum small-scale $N_{s,max}$. The number −5/3 indicates the spectral slope $\sigma^{-5/3}$ for frequency σ, −2 the spectral slope $\sigma^{-2}$. The 95% significance level is indicated by the small vertical bar and by the width of the two −2 slopes. After [67]

Whatever, the 3D mooring reveals the transition from squashed stratified turbulence having an aspect ratio of $\leq 0.5$ near the large-scale buoyancy frequency to fully developed turbulence of aspect ratio equal to 1 before coherence is lost around a frequency of about twice the maximum (resolved) small-scale buoyancy frequency.

## Discussion and Conclusions

Turbulence values are high in the lower 100 m above sloping topography (e.g., [8, 32]). They are 100–1000 times larger than observed in the open ocean, away from boundaries (e.g., [52, 31). Considering the rapid restratification process by the (sloshing or propagating) carrier waves, the turbulent mixing is found to be effective. Thus, the interplay between the large-scale internal waves and the small-scale waves near the buoyancy frequency acts to create both the diapycnal turbulent mixing and the isopycnal transport of the mixed waters into the interior. The T-string observed high mean turbulent diffusivity values $O(10^{-3} - 10^{-2})$ $m^2$ $s^{-1}$ are confirmed by various other Mid-Atlantic Ridge shipborne data (e.g., [68]) and Jim Ledwell's recent Mid-Atlantic Ridge tracer release experiments: These diffusivities are (observed to be) required to balance a near-bottom upslope motion.

Following Armi's [25] suggestion that about 3% of the ocean is occupied by such 100 m tall layer of large turbulence, the high mean turbulent diffusivities observed over sloping topography will yield an overall mean ocean-basin-interior diffusivity of $K_z \approx 1\text{–}3 \times 10^{-4}$ $m^2$ $s^{-1}$, sufficient to maintain the ocean stratification [3, 24]. Above particular steep seamount slopes of Mount Josephine (NE Atlantic Ocean) that are supercritical for internal tides, the local large-scale carrier wave, high local diffusivity values suggest a relatively narrow range of only 450 m depth interval sufficient to supply this overall ocean-basin-interior diffusivity if the turbulence observed over these particular slopes is extrapolated to other ocean topography [18]. This large turbulence above tidally supercritical slopes is confirmed by numerical modelling of Winters [19] and Sarkar (2016, pers. comm.). It supports earlier conjectures (e.g., [24, 25]) for the importance of sloping boundary mixing.

Previous and present data suggest that such mixing is quite universal, independent of forcing (carrier wave) mechanism (frequency), but strongly dependent on slope with respect to that of the carrier wave. The turbulence above sloping topography well (>300 m) below the summits of seamounts is determined by slope steepness and nonlinear wave evolution, but not by bottom-friction, and not necessarily by 'critical' internal tide reflection, internal hydraulic jumps or lee-wave generation. Lee-waves are estimated to carry about one-tenth of the energy of internal tides, although this may vary for certain locations [69]. Tides are not the only forcing mechanism, as turbulent overturns are also observed in seas like the Baltic and the Mediterranean Sea where tides are weak. Bottom slopes need not be 'critical' for sediment resuspension as suggested for the occurrence of intermediate nepheloid layers [70]: Vigorous bore-like motions have also been observed at a

variety of [tidally] non-critical slopes for sub-inertial motions (e.g., [23, 33]). Near-inertial shear, the largest internal wave shear outside internal tidal generation areas, is important for (high-frequency) internal wave breaking away from the bottom, in case shear-induced mixing is the dominant turbulence generation process. Thus, most internal wave—turbulence transitions seem associated with non-linear deformation of internal wave motions near local buoyancy frequencies.

The ocean interior is a much smoother linear-wave-like environment, but it too is in permanent motion rather than quiescent. This ocean in permanent motion is driven by surprisingly weak kinetic energy forcing of about 20% of the total energy presently used by mankind, about 500 times less than the heat flux transported in the ocean [3] and 25,000 times less than the solar energy received by the ocean. Man can maximally retrieve about 3% van the kinetic tidal energy or maximum 0.6% of his present-day demand with the notion that the present-day technology is not economically viable. In the hypothetical case that man were able to efficiently extract more tidal energy he would destroy the ocean stratification and with it ocean life, not only in the deep ocean but especially also in tidal inlets of nursery areas where currents are largest.

Of all the power of 100-m breaking waves above deep-ocean topography, while highly important for redistribution of sediment and for life e.g. by replenishing nutrients to cold-water coral mounds (e.g., [71]), which are found at depths where mineralization is relatively large as inferred from the seasonal oxygen minimum layer coinciding with nutrient maxima (e.g., [72]), very little is sensed at the surface. Therefore, in order to learn more about internal wave-turbulence processes it is mandatory to continue studying their characteristics in the deep sea and ocean, above sloping topography but especially also their extend into the interiors. Future instrumentation development should be directed to a truly four-dimensional, 3-D spatial plus temporal, resolution of the internal wave-turbulence motions to understand their intrinsic properties. Typical turn-over scales generated by KHI and frontal bores are between 1 and 100 m, whereas typical internal wave lengths are 100–1000 m. A small array with T-sensors a few meters apart would be useful to study internal wave—turbulence resolving the short spatial scales. A larger cubic hectometer array with T-sensors O(10 m) apart would be useful to study the statistical properties and internal wave propagation and will yield new insight in internal wave development. After all, deep-ocean sloping topography generates great surf!

**Acknowledgements** I greatly thank M. Laan, L. Gostiaux, A. Cimatoribus and F. Cyr for their discussions, collaboration in design and construction of NIOZ temperature sensors. NIOZ temperature sensors has been financed in part by NWO, the Netherlands Organization for Scientific Research.

## References


1. Gill, A. E. (1982). *Atmosphere-ocean dynamics* (p. 662). Orlando Fl, USA: Academic Press.
2. Peixoto, J. P., & Oort, A. H. (1992). *Physics of climate* (p. 520). Melville NY, USA: AIP-Press.
3. Munk, W., & Wunsch, C. (1998). Abyssal recipes II: Energetics of tidal and wind mixing. *Deep Sea Research Part I: Oceanographic Research Papers, 45,* 1977–2010.
4. van Haren, H., Maas, L., Zimmerman, J. T. F., Ridderinkhof, H., & Malschaert, H. (1999). Strong inertial currents and marginal internal wave stability in the central North Sea. *Geophysical Reseach Letters, 26,* 2993–2996.
5. Bell, T. H. (1975). Topographically generated internal waves in the open ocean. *Journal Geophysical Research, 80,* 320–327.
6. LeBlond, P. H., & Mysak, L. A. (1978). *Waves in the Ocean* (p. 602). New York, USA: Elsevier.
7. Morozov, E. G. (1995). Semidiurnal internal wave global field. *Deep Sea Research Part I: Oceanographic Research Papers, 42,* 135–148.
8. Eriksen, C. C. (1982). Observations of internal wave reflection off sloping bottoms. *Journal Geophysical Research, 87,* 525–538.
9. Thorpe, S. A. (1987). Current and temperature variability on the continental slope. *Philosophical Transactions of the Royal Society of London A, 323,* 471–517.
10. Davies, A. M., Xing, J. (2005). The effect of a bottom shelf front upon the generation and propagation of near-inertial internal waves in the coastal ocean. *Journal of Physical Oceanography, 35*, 976–990.
11. Turner, J. S. (1979). *Buoyancy effects in fluids* (p. 368). Cambridge, UK: Cambridge University Press.
12. Sharp, D. H. (1984). An overview of Rayleigh-Taylor instability. *Physica D, 12,* 3–18.
13. Marshall, J., & Schott, F. (1999). Open-ocean convection: Observations, theory and models. *Reviews of Geophysics, 37,* 1–64.
14. Li, S., & Li, H. (2006). Parallel AMR code for compressible MHD and HD equations. T-7, MS B284, Theoretical division, Los Alamos National Laboratory, http://math.lanl.gov/Research/Highlights/amrmhd.shtml.
15. Matsumoto, Y., & Hoshino, M. (2004). Onset of turbulence by a Kelvin-Helmholtz vortex. *Geophysical Reseach Letters, 31,* L02807. https://doi.org/10.1029/2003GL018195.
16. Inall, M. E., Rippeth, T. P., Griffiths, C. R., & Wiles, P. (2005). Evolution and distribution of TKE production and dissipation within stratified flow over topography. *Geophysical Reseach Letters, 32,* L08607. https://doi.org/10.1029/2004GL022289.
17. Klymak, J. M., Legg, S., & Pinkel, R. (2010). A simple parameterization of turbulent tidal mixing near supercritical topography. *Journal of Physical Oceanography, 40,* 2059–2074.
18. Cimatoribus, A. A., & van Haren, H. (2015). Temperature statistics above a deep-ocean sloping boundary. *Journal of Fluid Mechanics, 775,* 415–435.
19. Winters, K. B. (2015). Tidally driven mixing and dissipation in the boundary layer above steep submarine topography. *Geophysical Reseach Letters, 42,* 7123–7130. https://doi.org/10.1002/2015GL064676.
20. Dauxois, T., Didier, A., & Falcon, E. (2004). Observation of near-critical reflection of internal waves in a stably stratified fluid. *Physics of Fluids, 16,* 1936–1941.
21. Ivey, G. N., & Nokes, R. I. (1989). Vertical mixing due to the breaking of critical internal waves on sloping boundaries. *Journal of Fluid Mechanics, 204,* 479–500.
22. van Haren, H., Groenewegen, R., Laan, M., & Koster, B. (2005). High sampling rate thermistor string observations at the slope of Great Meteor Seamount. *Ocean Science, 1,* 17–28.
23. Hosegood, P., Bonnin, J., & van Haren, H. (2004). Solibore-induced sediment resuspension in the Faeroe-Shetland channel. *Geophysical Reseach Letters, 31,* L09301. https://doi.org/10.1029/2004GL019544.

24. Munk, W. (1966). Abyssal recipes. *Deep-Sea Research, 13,* 707–730.
25. Armi, L. (1979). Effects of variations in eddy diffusivity on property distributions in the oceans. *Journal of Marine Research, 37,* 515–530.
26. Garrett, C. (1990). The role of secondary circulation in boundary mixing. *Journal Geophysical Research, 95,* 3181–3188.
27. Ekman, V. W. (1905). On the influence of the Earth's rotation on ocean-currents. *Arkiv för Matematik, Astronomi och Fysik, 2*(11), 1–52.
28. Weatherly, G. L., & Martin, P. J. (1978). On the structure and dynamics of the oceanic bottom boundary layer. *Journal of Physical Oceanography, 8,* 557–570.
29. Dewey, R. K., Crawford, W. R., Gargett, A. E., & Oakey, N. S. (1987). A microstructure instrument for profiling oceanic turbulence in coastal bottom boundary layers. *Journal of Atmospheric and Oceanic Technology, 4,* 288–297.
30. van Haren, H., Oakey, N., Garrett, C. (1994). Measurements of internal wave band eddy fluxes above a sloping bottom. *Journal of Marine Research, 52*, 909–946.
31. Polzin, K. L., Toole, J. M., Ledwell, J. R., Schmitt, R. W. (1997). Spatial variability of turbulent mixing in the abyssal ocean. *Science, 276*, 93–96.
32. van Haren, H., & Gostiaux, L. (2012). Detailed internal wave mixing observed above a deep-ocean slope. *Journal of Marine Research, 70,* 173–197.
33. Klymak, J. M., & Moum, J. N. (2003). Internal solitary waves of elevation advancing on a shoaling shelf. *Geophysical Reseach Letters, 30,* 2045. https://doi.org/10.1029/2003GL017706.
34. Ferrari, R., Mashayek, A., McDougall, T. J., Nikurashin, M., & Campin, J. (2016). Turning ocean mixing upside down. *Journal of Atmospheric and Oceanic Technology, 46,* 2239–2261.
35. Tennekes, H., & Lumley, J. L. (1972). *A first course in turbulence* (p. 293). Cambridge, MA USA: MIT Press.
36. Thorpe, S. A. (1977). Turbulence and mixing in a Scottish loch. *Philosophical Transactions of the Royal Society of London A, 286,* 125–181.
37. Dillon, T. M. (1982). Vertical overturns: A comparison of Thorpe and Ozmidov length scales. *Journal Geophysical Research, 87,* 9601–9613.
38. Mater, B. D., Venayagamoorthy, S. K., St. Laurent, L., & Moum, J. N. (2015). Biases in Thorpe scale estimates of turbulence dissipation. Part I: Assessments from large-scale overturns in oceanographic data. *Journal of Physical Oceanography, 45*, 2497–2521.
39. Oakey, N. S. (1982). Determination of the rate of dissipation of turbulent energy from simultaneous temperature and velocity shear microstructure measurements. *Journal of Physical Oceanography, 12,* 256–271.
40. Osborn, T. R. (1980). Estimates of the local rate of vertical diffusion from dissipation measurements. *Journal of Physical Oceanography, 10,* 83–89.
41. Galbraith, P. S., & Kelley, D. E. (1996). Identifying overturns in CTD profiles. *Journal of Atmospheric and Oceanic Technology, 13,* 688–702.
42. Gargett, A. E., & Garner, T. (2008). Determining Thorpe scales from ship-lowered CTD density profiles. *Journal of Atmospheric and Oceanic Technology, 25,* 1657–1670.
43. Stansfield, K., Garrett, C., & Dewey, R. (2001). The probability distribution of the Thorpe displacement within overturns in Juan de Fuca Strait. *Journal of Physical Oceanography, 31,* 3421–3434.
44. van Haren, H., & Gostiaux, L. (2014). Characterizing turbulent overturns in CTD-data. *Dynamics of Atmospheres and Oceans, 66,* 58–76.
45. Fer, I., & Paskyabi, M. (2014). Autonomous ocean turbulence measurements using shear probes on a moored instrument. *Journal of Atmospheric and Oceanic Technology, 31,* 474–490.
46. Lohrmann, A., Hackett, B., & Røed, L. P. (1990). High resolution measurements of turbulence, velocity and stress using a pulse-to-pulse coherent sonar. *Journal of Atmospheric and Oceanic Technology, 7,* 19–37.
47. Rippeth, T. P., Williams, E., & Simpson, J. H. (2002). Reynolds stress and turbulent energy production in a tidal channel. *Journal of Physical Oceanography, 32,* 1242–1251.

48. Gemmrich, J. R., & van Haren, H. (2002). Internal wave band eddy fluxes in the bottom boundary layer above a continental slope. *Journal of Marine Research, 60,* 227–253.
49. van Haren, H., Laan, M., Buijsman, D.-J., Gostiaux, L., Smit, M. G., & Keijzer, E. (2009). NIOZ3: Independent temperature sensors sampling yearlong data at a rate of 1 Hz. *IEEE Journal of Oceanic Engineering, 34,* 315–322.
50. IOC, SCOR, & IAPSO. (2010). The international thermodynamic equation of seawater—2010: Calculation and use of thermodynamic properties. Intergovernmental Oceanographic Commission, Manuals and Guides No. 56, UNESCO, Paris, France, p. 196
51. van Haren, H., Greinert, J. (2016). Turbulent high-latitude oceanic intrusions – details of non-smooth apparent isopycnal transport West of Svalbard. *Ocean Dynamics, 66*, 785–794.
52. Gregg, M. C. (1989). Scaling turbulent dissipation in the thermocline. *Journal Geophysical Research, 94,* 9686–9698.
53. Alford, M. H., & Pinkel, R. (2000). Observations of overturning in the thermocline: The context of ocean mixing. *Journal of Physical Oceanography, 30,* 805–832.
54. Marmorino, G. O. (1987). Observations of small-scale mixing processes in the seasonal thermocline. Part II: Wave breaking. *Journal of Physical Oceanography, 17,* 1348–1355.
55. van Haren, H., & Gostiaux, L. (2009). High-resolution open-ocean temperature spectra. *Journal Geophysical Research, 114,* C05005. https://doi.org/10.1029/2008JC004967.
56. Munk, W. (1981). Internal waves and small-scale processes. In B. A. Warren & C. Wunsch (Eds.), *Evolution of physical oceanography* (pp. 264–291). Cambridge MA, USA: MIT Press.
57. Cyr, F., & van Haren, H. (2016). Observations of small-scale secondary instabilities during the shoaling of internal bores on a deep-ocean slope. *Journal of Physical Oceanography, 46,* 219–231.
58. Geyer, W. R., Lavery, A. C., Scully, M. E., & Trowbridge, J. H. (2010). Mixing by shear instability at high Reynolds number. *Geophysical Reseach Letters, 37,* L22607. https://doi.org/10.1029/2010GL045272.
59. van Haren, H. (2006). Nonlinear motions at the internal tide source. *Geophysical Reseach Letters, 33,* L11605. https://doi.org/10.1029/2006GL025851.
60. van Haren, H., Cimatoribus, A. A., Gostiaux, L. (2015). Where large deep-ocean waves break. *Geophysical Research Letters, 42*, 2351–2357, https://doi.org/10.1002/2015GL063329.
61. van Haren, H. (2017). Exploring the vertical extent of breaking internal wave turbulence above deep-sea topography. *Dynamics of Atmospheres and Oceans, 77,* 89–99.
62. van Haren, H., Gostiaux, L., Morozov, E., & Tarakanov, R. (2014). Extremely long Kelvin-Helmholtz billow trains in the Romanche Fracture Zone. *Geophysical Reseach Letters, 41,* 8445–8451. https://doi.org/10.1002/2014GL062421.
63. Thorpe, S. A. (1973). Experiments on instability and turbulence in a stratified shear flow. *Journal of Fluid Mechanics, 61,* 731–751.
64. Klaassen, G. P., & Peltier, W. R. (1985). The onset of turbulence in finite-amplitude Kelvin-Helmholtz billow. *Journal of Fluid Mechanics, 155,* 1–35.
65. Woods, J. D. (1968). Wave-induced shear instability in the summer thermocline. *Journal of Fluid Mechanics, 32,* 791–800.
66. Moum, J. M., Farmer, D. M., Smyth, W. D., Armi, L., & Vagle, S. (2003). Structure and generation of turbulence at interfaces strained by internal solitary waves propagating shoreward over the continental shelf. *Journal of Physical Oceanography, 33,* 2093–2112.
67. van Haren, H., Cimatoribus, A. A., Cyr, F., & Gostiaux, L. (2016). Insights from a 3-D temperature sensors mooring on stratified ocean turbulence. *Geophysical Reseach Letters, 43,* 4483–4489. https://doi.org/10.1002/2016GL068032.
68. Thurnherr, A. M., Richards, K. J., German, C. R., Lane-Serff, G. F., & Speer, K. G. (2002). Flow and mixing in the Rift Valley of the Mid-Atlantic Ridge. *Journal of Physical Oceanography, 32,* 1763–1778.
69. Melet, A., Hallberg, R., Legg, S., & Nikurashin, M. (2014). Sensivity of the ocean state to lee-wave driven mixing. *Journal of Physical Oceanography, 40,* 900–921.
70. Cacchione, D. A., & Drake, D. E. (1986). Nepheloid layers and internal waves over continental shelves and slopes. *Geo-Marine Letters, 16,* 147–152.

71. Cyr, F., van Haren, H., Mienis, F., Duineveld, G., & Bourgault, D. (2016). On the influence of cold-water coral mound size on flow hydrodynamics, and vice-versa. *Geophysical Reseach Letters, 43,* 775–783. https://doi.org/10.1002/2015GL067038.
72. Tsuchiya, M., Talley, L. D., & McCartney, M. S. (1992). An eastern Atlantic section from Iceland southward across the equator. *Deep Sea Research Part A. Oceanographic Research Papers, 39,* 1885–1917.